Applied Mathematical Modelling 94 (2021) 68–86

Contents lists available at ScienceDirect

Applied Mathematical Modelling

journal homepage: www.elsevier.com/locate/apm

Multi-phase-field modelling of the elastic and buckling behaviour of laminates with ply cracks

Duc Hong Doan[a,b,*], Thom Van Do[c,**], Nguyen Xuan Nguyen[d], Pham Van Vinh[c], Nguyen Thoi Trung[a,b]

[a] Division of Computational Mathematics and Engineering, Institute for Computational Science, Ton Duc Thang University, Ho Chi Minh City, Vietnam
[b] Faculty of Civil Engineering, Ton Duc Thang University, Ho Chi Minh City, Vietnam
[c] Faculty of Mechanical Engineering, Le Quy Don Technical University, Hanoi, Viet Nam
[d] Department of Mathematics, Mechanics and Informatics, University of Science, Vietnam National University, Hanoi, Vietnam

ARTICLE INFO

Article history:
Received 4 September 2020
Revised 25 December 2020
Accepted 30 December 2020
Available online 12 January 2021

Keywords:
Buckling
Multiple transverse ply cracking laminates
Finite element method

ABSTRACT

The phase-field theory is a well-known mathematical model for solving interface problems, including crack problems in fracture mechanics. In this study, the formula is derived by variational approaches based on the Reissner-Mindlin plate kinematics and the multi-phase-field theory for simulation of the buckling phenomenon in cracked laminates. Phase-field parameters are defined independently in different plies of laminate to capture the crack behavior of each ply. Simulation is carried out to numerically investigate the stiffness reduction and buckling behavior of transverse cracked laminated composite plates. This paper focuses on the consideration of laminated composite plates, which have a crack in each layer. Therefore, this work is more complicated than the case of the plate has one crack throughout the plate thickness. The significant advancement of the phase-field approach for laminated composite plates with complex crack geometries is demonstrated.

1. Introduction

Composite laminates are widely employed in various engineering fields because they have many advantages such as high strength-to-weight and stiffness-to-weight ratios, saving energy, and low production cost. Many of their applications can be mentioned such as aerospace, shipbuilding, automotive industry, wind power, and so on. In fact, these composite structures are always subjected to various types of external loads with high intensity. However, they are made of different reinforced materials and fibers, and therefore often appear cracks, especially cracks that do not penetrate the thickness of the structure and along the angle-ply. The characteristics of this type of crack are often difficult to identify, so if they extend, the performing ability of the structure can be reduced. The analysis of cracked structures is a significant challenge for scientists. To model cracks, in general, some highlight approaches can be used such as extended finite element method (XFEM), extended isogeometric analysis (XIGA), meshfree method, generalized differential quadrature, and so on. For the XFEM approach, it is based on the discrete method of finite element method (FEM), the shape can be enriched in a location,

* Corresponding author at: Division of Computational Mathematics and Engineering, Institute for Computational Science, Ton Duc Thang University, Ho Chi Minh City, Vietnam.
** Corresponding author.
E-mail addresses: doanhongduc@tdtu.edu.vn (D.H. Doan), thom.dovan@lqdtu.edu.vn (T. Van Do).

https://doi.org/10.1016/j.apm.2020.12.038
0307-904X/

thus, it can be used to solve simple crack problems. However, the computational cost of this approach will increase rapidly for the problems with multiple cracks in different surfaces of the structure. The isogeometric analysis (IGA) is a method that uses the splines function to represent the geometry, which can give an approximation. The XIGA is developed from the IGA and some functions around the discontinuous domain, so it can also simulate cracks. The meshfree method is based on discontinuity through the crack of the displacement field and a singular behavior of the stresses around the crack, thus, this method also can be employed to analyze the problems related to cracks. The mentioned methods have been applied by scientists in analyzing problems related to static and dynamic cracks [1,2,21,28,29]. Amir and Soheil [2] used the XFEM to research the linear buckling behavior of cracked uni-layer composite plates based on the 8-node element. The laminated plates with cracks were also researched by Seifi and Ranjbaran [3], the buckling problem of these plates were carried out by using the generalized differential quadrature method and domain decomposition technique. Amit [4] explored the nonlinear buckling response of damaged laminated composite plates based on the finite element method and layerwise plate theory. However, most of these approaches analyzed cracks throughout the thickness of structures, including some published works that computed composite plates considering such cracks. This sometimes does not properly reflect the working processes of multi-layered composite structures, because these structures are made up of different reinforcement materials, and arranged in separate layers. It is possible that cracks can appear in each layer during fabrication, or during the working process, cracks in each layer will appear without penetrating the plate thickness. The appearance of cracks has a significant impact on the efficiency of using them, so the calculation study for these structures is an urgent requirement from reality.

Recently, there have been several computational models for cracks that do not penetrate the thickness of the structures [5-8]. Li et al. [6] applied Layerwise theories theory and XFEM to analyze laminated composite plates with the delamination phenomenon and the cracks occupied in a part of the thickness of the structure. By using the block elements and Layerwise theory, Lu et al. [7] investigated the displacement of the cracked sandwich plate. Li et al. [8] then used Layerwise theories and XFEM theory to carry out the free and forced vibration analyses of cracked FGM plates. Several works have also mentioned the investigations of beam and plate composite structures with many cracks [9,10], Li et al. [9] explored the mechanical behavior of composite beam with multiple cracks that were affected by impact loads. Yuan et al. [10] applied a novel trans-scale solution to study composite plates with multiple cracks.

The phase-field method is a new approach to deal with fracture problems, the advantage of this method is to change the crack domain (discontinuous domain) to become a continuous domain through a phase-field variable. This variable is continuously smooth from 0 to 1 corresponding to the state of the material from destructive to non-destructive. Since its inception, it has been highly appreciated by scientists and is widely applied to analyze 2D and 3D cracked structures [15,16,18,19,21]. For beam and plate structures, there is just one publication applying this theory to explore the mechanical behavior of the Euler- Bernoulli beam with multiple cracks subjected to bending load [11]. Thom et al. and Duc et al. also applied phase-field theory to investigate cracked plates with different plate theories [20,22-25]. However, the previous publications of the authors only considered the cracks, which were throughout the plate thickness, so there are no studies to simulate the response of plates with multi cracks, in which each crack locates in one part of the thickness direction. On the other hand, for multilayered composite plates, each layer with a different reinforcement angle may appear cracks in only each layer, therefore, the investigation of mechanical responses of these structures is very interesting, which plays an important role in using, designing, and studying these structures in engineering practice.

As mentioned above, due to the combination of many different materials, structures made of composite materials may crack in the direction of the angle-plies, and for this reason, several studies have been conducted with laminated composite structures that have cracks along these angles [12,13,14]. Han et al. [12] used polynomial (second-order) to present the displacement of the open crack, thereby the stress around the crack can be described. Singh and Talreja [13] studied the mechanical behavior of laminated composite plates under tensile loads, which focused on the deformation and stiffness degradation in cracks by using analytical formulas and finite element models, which are integrated into Ansys software. Carraro and Quaresimin [14] used an analytical approach to examine the decrease of stiffness in perpendicular directions to the crack of the laminated composite structures when one and more cracks appear in the layers.

Recently, there have been some publications used high order phase-field and multi-phase-field to investigate cracked structures. Peng et al. [30] employed a novel phase-field model to study progressive failure in composite laminates under tension load. Udit et al. [31] proposed a cohesive phase-field model to simulate intra-laminar fracture in fiber-reinforced composites. Wu et al. [32] used a fourth-order phase field and an efficient gradient smoothing meshfree to model brittle fractures. Chen and his co-workers [33] studied crack kinking and zig-zag crack propagation based on a higher-order phase-field. Ma and Sun [34] employed multi-phase-field fracture models to solve two phase-field models designed and simulate crack growth of strongly anisotropic materials in the brittle regime. Dean et al. [35] also used a multi phase-field to consider triggering intra-laminar cracking in long fiber-reinforced composites. However, these studies have not provided any models and approaches to analyze the buckling and free vibration problems, which are common issues in practice. Therefore, in this work, the phase-field theory is employed to investigate the multi-crack plate based on Mindlin plate theory, each layer has one crack through the thickness of the layer according to the angle-ply and not through the total thickness of the plate. To develop this theory, many phase-field variables are used, each one describes the crack of the layer.

This paper is divided into 4 sections. Section 2 presents briefly some finite element formulations of laminated composite plates based on the first-order shear deformation theory. The phase-field is employed and shown clearly in Section 2 to describe the appearance of cracks in the structure. Section 3 is about numerical results and discussions of laminated composite plates. Some highlight conclusions are listed in section 4.

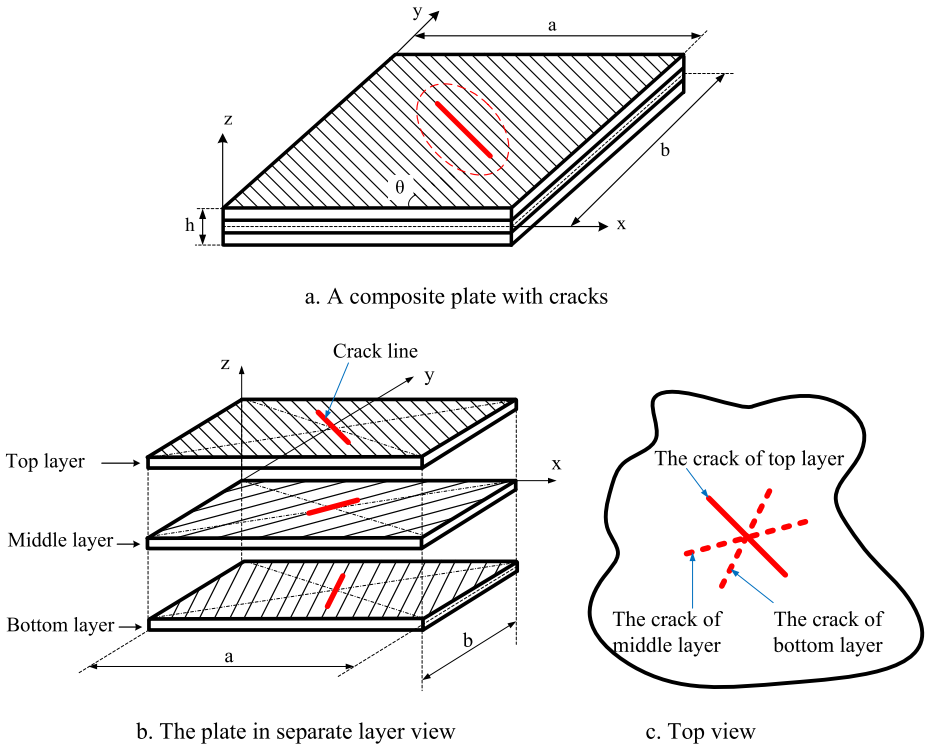

Fig. 1. The geometric model of a cracked laminated plate.

2. Formulation for composite plates based on first-order shear deformation theory

Consider a composite plate under a Cartesian coordinate system with the thickness h as shown in Fig. 1.

In this paper, a laminated plate with different layers as shown in Fig. 1 is considered. Each layer of the plate has one crack along its angle-ply and throughout the layer thickness. In order to describe all cracks, multi-phase-field theory is employed with different phase-filed variables s_q (q=1-N, N is the number of layers), each variable s_q represents the crack of layer q.

As the plate is under a compressive load in the mid-plane, the energy of the structure including the energy of each cracked layer is expressed as follows [37]:

$$\begin{aligned}\Pi_b^p = &\frac{1}{2}\int_\Omega\int_{z_{q-1}}^{z_q} s_q^2\varepsilon_{ij}C_{ijkl}^q\varepsilon_{kl}dzd\Omega + \frac{1}{2}\int_\Omega\int_{z_{q-1}}^{z_q} s_q^2\nabla^T w\hat{\sigma}^0\nabla w dzd\Omega\\ &+\frac{1}{2}\int_\Omega\int_{z_{q-1}}^{z_q} s_q^2\nabla^T\phi_x\hat{\sigma}^0\nabla\phi_x z_q^2 dzd\Omega + \frac{1}{2}\int_\Omega\int_{z_{q-1}}^{z_q} s_q^2\nabla^T\phi_y\hat{\sigma}^0\nabla\phi_y z_q^2 dzd\Omega\\ &+\int_\Omega\int_{z_{q-1}}^{z_q} G_C^q\left[\frac{(1-s_q)^2}{4l} + l|\nabla s_q|^2\right]dzd\Omega\end{aligned} \tag{1}$$

where the strains are the same in each layer and defined as:

$$\varepsilon_{ij} = \frac{1}{2}\left(u_{i,j} + u_{j,i}\right) \tag{2}$$

and the Cauchy stress tensor σ_{ij} in layer q is computed from strain as [38]

$$\sigma_{ij}^q = C_{ijkl}^q\varepsilon_{kl} \tag{3}$$

the prebuckling stress tensor is

$$\hat{\sigma}^0 = \begin{bmatrix}\sigma_x^0 & \tau_{xy}^0\\ \tau_{xy}^0 & \sigma_y^0\end{bmatrix} \tag{4}$$

In this paper, the phase-field approach presented by Bourdin et al. [19] is used, the crack is modeled by a narrow region and controlled by the phase-field variable s_q which gets value from 0 (total broken) to 1 (unbroken). When analyzing the cracked plate, the potential function of each ply is multiplied by the phase-field variable s_q. In detail, in the non-cracked

area of each ply (s_q=1), the energy does not change. In contrast, at the cracked area, due to the phase-field variable s_q varies smoothly from 1 to 0 corresponding to the rear and the center of the crack, respectively, the energy of this area changes as a function of the phase-field variable. At the same time, the energy released at the cracked area will be added to the whole energy of the system. This part of the energy is the main reason leading the cracked ply to be softer in comparison with the plate without any cracks [18,19,29]. Therefore, in practice, the energy function of the cracked ply is most likely similar to that of the ply without any cracks by using the phase-field variables s_q, so the accuracy of the present approach will be enhanced. The interpolation of variable s_q for each element in the cracked area is carried out similarly to the interpolation of other degrees of freedom of the element, which makes the cracked region a continuous zone, hence, it is convenient for computing. Note that in Eq. (1) for the problem of cracked plates under compression loads, the crack will be closed, the phase-field model proposed in this work has not shown this property clearly. However, according to the group of published works by the author [20,22] has shown that when comparing this model with other computational methods as well as comparing with experiments, it is found that the proposed model is still for acceptable results. Thereby, it can be seen that, for the buckling problems of plates under the small deformation condition, the effect of the cracking characteristic when subjected to the compressive load is not obvious and can be ignored. Therefore, to keep the solution neat and avoid cumbersome calculation, the authors still use this model to calculate like the references [36,39], which is also the model used by other authors to investigate the cracked structures [39]. The authors also found that in some cases such as post-buckling problems, in which large strain is taken into account, Eq. (1) needs to be adjusted to better accommodate cracking closed when subjected to compression loads, which has been proposed by several other authors [37].

Derived from phase-field theory, G_C^q is the critical energy release rate or surface energy in Griffith's theory and l is a positive regularization constant to regulate the size of the fracture zone. The effect of the parameter l on the critical buckling load was investigated and indicated details in [22], where l varied from a/800 to a/100, the value of l had a small effect on critical loads, therefore, in this study $l = a/200$ was chosen.

Based on Mindlin plate theory, the displacement field is expressed as:

$$\begin{aligned} u(x,y,z) &= u_0(x,y) + z\phi_x(x,y) \\ v(x,y,z) &= v_0(x,y) + z\phi_y(x,y) \\ w(x,y,z) &= w_0(x,y) \end{aligned} \tag{5}$$

where u,v,w are the displacement components in the x, y, z axes, respectively. φ_x,φ_y are the transverse normal rotations in the xz- and yz- planes; u_0,v_0,w_0 are displacements of the middle surface.

At this time, the energy Eq. (1) will be written in the following form:

$$\begin{aligned} \Pi_b^p(\boldsymbol{u}, s) &= \frac{1}{2}\int_\Omega \int_{z_{q-1}}^{z_q} s_q^2\left(\boldsymbol{\varepsilon}_p^T\mathbf{A}_q\boldsymbol{\varepsilon}_p + \boldsymbol{\varepsilon}_p^T\mathbf{B}_q\boldsymbol{\varepsilon}_b + \boldsymbol{\varepsilon}_b^T\mathbf{B}_q\boldsymbol{\varepsilon}_p + \boldsymbol{\varepsilon}_b^T\mathbf{D}_q\boldsymbol{\varepsilon}_b + \boldsymbol{\gamma}_s^T H_q\boldsymbol{\gamma}_s\right)d\Omega \\ &+ \frac{1}{2}\int_\Omega \int_{z_{q-1}}^{z_q} s_q^2\nabla^T w\hat{\sigma}^0\nabla w dz d\Omega + \frac{1}{2}\int_\Omega \int_{z_{q-1}}^{z_q} s_q^2\nabla^T\phi_x\hat{\sigma}^0\nabla\phi_x z_q^2 dz d\Omega \\ &+ \frac{1}{2}\int_\Omega \int_{z_{q-1}}^{z_q} s_q^2\nabla^T\phi_y\hat{\sigma}^0\nabla\phi_y z_q^2 dz d\Omega + \int_\Omega \int_{z_{q-1}}^{z_q} G_C^q\left[\frac{(1-s_q)^2}{4l} + l|\nabla s_q|^2\right]dz d\Omega \\ &= \left\{\int_\Omega s_q^2\Psi_q(\boldsymbol{u})d\Omega + \int_\Omega \int_{z_{q-1}}^{z_q} G_C^q\left[\frac{(1-s_q)^2}{4l} + l|\nabla s_q|^2\right]dz d\Omega\right\} \end{aligned} \tag{6}$$

where the vectors $\boldsymbol{\varepsilon}_p$ and $\boldsymbol{\varepsilon}_b$contain a membrane, bending and transverse strain, respectively.

$$\boldsymbol{\varepsilon}_p = \begin{Bmatrix} u_{0,x} \\ v_{0,y} \\ u_{0,y} + v_{0,x} \end{Bmatrix} \boldsymbol{\varepsilon}_b = \begin{Bmatrix} \phi_{x,x} \\ \phi_{y,y} \\ \phi_{x,y} + \phi_{y,x} \end{Bmatrix} \boldsymbol{\gamma}_s = \begin{Bmatrix} \phi_x + w_{0,x} \\ \phi_y + w_{0,y} \end{Bmatrix} \tag{7}$$

where the matrices $\boldsymbol{A_q}$,$\boldsymbol{B_q}$,$\boldsymbol{D_q}$, and $\boldsymbol{H_q}$ are respectively the extensional, bending-extensional coupling, bending stiffness coefficients and explicitly, which are given by

$$\mathrm{A}_q = \begin{bmatrix} A_{11} & A_{12} & A_{16} \\ A_{12} & A_{22} & A_{26} \\ A_{16} & A_{26} & A_{66} \end{bmatrix}_q ; \mathrm{B}_q = \begin{bmatrix} B_{11} & B_{12} & B_{16} \\ B_{12} & B_{22} & B_{26} \\ B_{16} & B_{26} & B_{66} \end{bmatrix}_q ; \mathbf{D}_q = \begin{bmatrix} D_{11} & D_{12} & D_{16} \\ D_{12} & D_{22} & D_{26} \\ D_{16} & D_{26} & D_{66} \end{bmatrix}_q$$

$$\boldsymbol{H}_q = \begin{bmatrix} \mathrm{H}_{44} & 0 \\ 0 & \mathrm{H}_{55} \end{bmatrix}_q \tag{8}$$

with

$$A_{ij} = \sum_{q=1}^{N}\bar{Q}_{ij}\left(z_q - z_{q-1}\right); B_{ij} = \frac{1}{2}\sum_{q=1}^{N}\bar{Q}_{ij}\left(z_q^2 - z_{q-1}^2\right); D_{ij} = \frac{1}{3}\sum_{q=1}^{N}\bar{Q}_{ij}\left(z_q^3 - z_{q-1}^3\right); i,j = 1,2,6$$

$$H_{ij} = \frac{5}{6}\sum_{q=1}^{N}\bar{Q}_{ij}\left(z_q - z_{q-1}\right); i,j = 4,5 \tag{9}$$

herein the quantities $\bar{Q}_{ij}$ are determined from the fiber direction θ, Young's modulus is parallel to and perpendicular to the orientation of the fibers E_1,E_2, shear modulus G_{12}, Poisson's ratios ν_{12},ν_{21} are as in reference [17].

The first variation of the functional $\Pi_b^p(\boldsymbol{u}, s)$ is given by

$$\begin{cases} \delta\Pi_b^p(\mathbf{u}, s, \delta\mathbf{u}) = 0 \\ \delta\Pi_b^p(\mathbf{u}, s, \delta s) = 0 \end{cases} \tag{10}$$

and then, the formulations for pre-buckling analyses of the cracked plate are expressed as

$$\begin{cases} \int_\Omega \int_{z_{q-1}}^{z_q} s_q^2\left(\boldsymbol{\varepsilon}_p^T\mathbf{A}_q\boldsymbol{\varepsilon}_p + \boldsymbol{\varepsilon}_p^T\mathbf{B}_q\boldsymbol{\varepsilon}_b + \boldsymbol{\varepsilon}_b^T\mathbf{B}_q\boldsymbol{\varepsilon}_p + \boldsymbol{\varepsilon}_b^T\mathbf{D}_q\boldsymbol{\varepsilon}_b + \boldsymbol{\gamma}_s^T H_q\boldsymbol{\gamma}_s\right)d\Omega \\ + \int_\Omega \int_{z_{q-1}}^{z_q} s_q^2\nabla^T w\hat{\sigma}^0\nabla(\delta w)dzd\Omega + \int_\Omega \int_{z_{q-1}}^{z_q} s_q^2\nabla^T\phi_x\hat{\sigma}^0\nabla(\delta\phi_x)z_q^2dzd\Omega \\ + \int_\Omega \int_{z_{q-1}}^{z_q} s_q^2\nabla^T\phi_y\hat{\sigma}^0\nabla(\delta\phi_y)z_q^2dzd\Omega = 0 \\ \int_\Omega 2s_q\Psi_q(\boldsymbol{u})\delta s_q d\Omega + \int_\Omega \int_{z_{q-1}}^{z_q} 2G_C^q\left[\frac{(1-s_q)\delta s_q}{4l} + l\nabla s_q\nabla(\delta s_q)\right]dzd\Omega = 0 \end{cases} \tag{11}$$

For the fracture problem, each node consists of displacement degrees and phase-field variables, when dividing the calculated domain into elements with n nodes, interpolation $u_i$and phase-field variable s at an internal point of the element according to the nodal displacements $\mathrm{u}_{ie} = \{u_{0i}, v_{0i}, w_{0i}, \varphi_{xi}, \varphi_{yi}\}^T$ and s_i at the nodes of the element is performed.

$$u_0 = \sum_{i=1}^n N_i u_{0i};\ v_0 = \sum_{i=1}^n N_i v_{0i};\ \phi_x = \sum_{i=1}^n N_i\phi_{xi} \tag{12}$$

$$\phi_y = \sum_{i=1}^n N_i\phi_{yi};\ w_0 = \sum_{i=1}^n N_i^w w_{0i};\ s_q = \sum_{i=1}^n N_i^q s_i \tag{13}$$

where N_i are the shape functions of the quadratic polynomial, N_i^w are the shape functions of the third-degree polynomial, and $N_i^q$are the shape functions of the first-degree polynomial. Note that in this work, to avoid the shear locking phenomenon, different shape functions are used for displacement components and phase-field variables to obtain the best convergence.

Then:

$$\boldsymbol{\varepsilon}_p = \mathrm{B}_1\mathrm{u}_e;\ \boldsymbol{\varepsilon}_b = \mathrm{B}_2\mathrm{u}_e;\ \boldsymbol{\gamma}_s = \mathrm{B}_3\mathrm{u}_e;\ w_0 = \mathrm{B}_4\mathrm{u}_e;\ \frac{\partial w_0}{\partial x} = \mathrm{B}_5\mathrm{u}_e;\ \frac{\partial w_0}{\partial y} = \mathrm{B}_6\mathrm{u}_e \tag{14}$$

$$\frac{\partial\phi_x}{\partial x} = \mathrm{B}_7\mathrm{u}_e;\ \frac{\partial\phi_x}{\partial y} = \mathrm{B}_8\mathrm{u}_e;\ \frac{\partial\phi_y}{\partial x} = \mathrm{B}_9\mathrm{u}_e;\ \frac{\partial\phi_y}{\partial y} = \mathrm{B}_{10}\mathrm{u}_e;\ \nabla s_q = \mathrm{B}_{11}^q\mathrm{s}_{qe} \tag{15}$$

where $\boldsymbol{B}_i$ are differential matrices of shape functions, they are calculated as:

$$\mathrm{B}_1 = \sum_{i=1}^n \begin{bmatrix} \frac{\partial N_i}{\partial x} & 0 & 0 & 0 & 0 \\ 0 & \frac{\partial N_i}{\partial y} & 0 & 0 & 0 \\ \frac{\partial N_i}{\partial y} & \frac{\partial N_i}{\partial x} & 0 & 0 & 0 \end{bmatrix};\ \mathrm{B}_2 = \sum_{i=1}^n \begin{bmatrix} 0 & 0 & 0 & \frac{\partial N_i}{\partial x} & 0 \\ 0 & 0 & 0 & 0 & \frac{\partial N_i}{\partial y} \\ 0 & 0 & 0 & \frac{\partial N_i}{\partial y} & \frac{\partial N_i}{\partial x} \end{bmatrix} \tag{16}$$

$$\mathrm{B}_3 = \sum_{i=1}^n \begin{bmatrix} 0 & 0 & \frac{\partial N_i}{\partial x} & N_i & 0 \\ 0 & 0 & \frac{\partial N_i}{\partial y} & 0 & N_i \end{bmatrix};\ \mathrm{B}_4 = \sum_{i=1}^n \begin{bmatrix} 0 & 0 & N_i^w & 0 & 0 \end{bmatrix} \tag{17}$$

$$\mathrm{B}_5 = \sum_{i=1}^n \begin{bmatrix} 0 & 0 & \frac{\partial N_i^w}{\partial x} & 0 & 0 \end{bmatrix};\ \mathrm{B}_6 = \sum_{i=1}^n \begin{bmatrix} 0 & 0 & \frac{\partial N_i^w}{\partial y} & 0 & 0 \end{bmatrix} \tag{18}$$

$$\mathrm{B}_7 = \sum_{i=1}^n \begin{bmatrix} 0 & 0 & 0 & \frac{\partial N_i}{\partial x} & 0 \end{bmatrix};\ \mathrm{B}_8 = \sum_{i=1}^n \begin{bmatrix} 0 & 0 & 0 & \frac{\partial N_i}{\partial y} & 0 \end{bmatrix} \tag{19}$$

$$\mathrm{B}_9 = \sum_{i=1}^n \begin{bmatrix} 0 & 0 & 0 & 0 & \frac{\partial N_i}{\partial x} \end{bmatrix};\ \mathrm{B}_{10} = \sum_{i=1}^n \begin{bmatrix} 0 & 0 & 0 & 0 & \frac{\partial N_i}{\partial y} \end{bmatrix};\ \mathrm{B}_{11}^q = \sum_{i=1}^n \begin{bmatrix} \frac{\partial N_i^q}{\partial x} \\ \frac{\partial N_i^q}{\partial y} \end{bmatrix} \tag{20}$$

Since then, Eq. (11) is written in the matrix form as follows:

$$\int_\Omega \mathrm{s}_{qe}^T\left\{\int_{z_{q-1}}^{z_q} 2\left(N_s^q\right)^T\Psi_q(\boldsymbol{u})N_s^q dz\right\}\mathrm{s}_{qe}d\Omega + \int_\Omega\int_{z_{q-1}}^{z_q} 2G_C^q\left[\frac{\left(N_s^q\mathrm{s}_{qe} - \mathrm{s}_{qe}^T\left(N_s^q\right)^T N_s^q\mathrm{s}_{qe}\right)}{4l} + \mathrm{s}_{qe}^T l\left(\mathrm{B}_{11}^q\right)^T\mathrm{B}_{11}^q\right]dzd\Omega = 0 \tag{21a}$$

$$\left(\mathbf{K}^e + \lambda_{cr}\mathbf{K}_G^e\right)\boldsymbol{u}_e = 0 \tag{21b}$$

in which, the element stiffness matrix $\mathbf{K}^e$, geometric element stiffness matrix $\mathbf{K}_G^e$, and element nodal displacement vector $\boldsymbol{u}_e$ are defined as:

$$\mathbf{K}^e = \int_\Omega \sum_{q=1}^{3} s_q^2\left(\mathrm{B}_1^T\mathbf{A}_q\mathrm{B}_1^T + \mathrm{B}_1^T\mathbf{B}_q\mathrm{B}_2^T + \mathrm{B}_2^T\mathbf{B}_q\mathrm{B}_1 + \mathrm{B}_2^T\mathbf{D}_q\mathrm{B}_2 + \mathrm{B}_3^T\mathrm{H}_q\mathrm{B}_3\right)d\Omega$$

$$\mathbf{K}_G^e = \int_\Omega \sum_{q=1}^{3}\left(z_q - z_{q-1}\right)s_q^2\left[\mathrm{B}_5^T\mathrm{B}_6^T\right]\hat{\sigma}^0[\mathrm{B}_5\mathrm{B}_6]d\Omega + \int_\Omega \sum_{q=1}^{3}\frac{1}{3}\left(z_q^3 - z_{q-1}^3\right)s_q^2\left[\mathrm{B}_7^T\mathrm{B}_8^T\right]\hat{\sigma}^0[\mathrm{B}_7\mathrm{B}_8]d\Omega$$
$$+ \int_\Omega \sum_{q=1}^{3}\frac{1}{3}\left(z_q^3 - z_{q-1}^3\right)s_q^2\left[\mathrm{B}_9^T\mathrm{B}_{10}^T\right]\hat{\sigma}^0[\mathrm{B}_9\mathrm{B}_{10}]d\Omega$$

$$\mathrm{u}_e = \sum_{i=1}^{n}\mathrm{u}_{ie} \tag{22}$$

Note that Eq. (21a) could be written in the following form:

$$\mathrm{s}_{qe}^T\left\{\int_{z_{q-1}}^{z_q}\int_\Omega 2\left(N_s^q\right)^T\Psi_q(\boldsymbol{u})N_s^q d\Omega dz\right\}\mathrm{s}_{qe} + \mathrm{s}_{qe}^T\left\{\int_{z_{q-1}}^{z_q}\int_\Omega 2G_C^q\left[\frac{-\left(N_s^q\right)^T N_s^q}{4l} + l\left(\mathrm{B}_{11}^q\right)^T\mathrm{B}_{11}^q\right]d\Omega dz\right\}\mathrm{s}_{qe}$$
$$+\left\{\int_{z_{q-1}}^{z_q}\int_\Omega 2G_C^q\left[\frac{N_s^q}{4l}\right]dzd\Omega\right\}\mathrm{s}_{qe} = 0 \tag{23}$$

or in the short form as:

$$\mathrm{s}_{qe}^T\left\{\int_{z_{q-1}}^{z_q}\int_\Omega 2\left(N_s^q\right)^T\Psi_q(\boldsymbol{u})N_s^q d\Omega dz\right\} + \mathrm{s}_{qe}^T\left\{\int_{z_{q-1}}^{z_q}\int_\Omega 2G_C^q\left[\frac{-\left(N_s^q\right)^T N_s^q}{4l} + l\left(\mathrm{B}_{11}^q\right)^T\mathrm{B}_{11}^q\right]d\Omega dz\right\}$$
$$= -\left\{\int_{z_{q-1}}^{z_q}\int_\Omega 2G_C^q\left[\frac{N_s^q}{4l}\right]dzd\Omega\right\} \tag{24}$$

For the whole structure, we have the following general equation:

$$\sum_e\left(\mathrm{s}_{qe}^T\left\{\int_{z_{q-1}}^{z_q}\int_\Omega 2\left(N_s^q\right)^T\Psi_q(\boldsymbol{u})N_s^q d\Omega dz\right\} + \mathrm{s}_{qe}^T\left\{\int_{z_{q-1}}^{z_q}\int_\Omega 2G_C^q\left[\frac{-\left(N_s^q\right)^T N_s^q}{4l} + l\left(\mathrm{B}_{11}^q\right)^T\mathrm{B}_{11}^q\right]d\Omega dz\right\}\right)$$
$$= -\sum_e\left\{\int_{z_{q-1}}^{z_q}\int_\Omega 2G_C^q\left[\frac{N_s^q}{4l}\right]dzd\Omega\right\} \tag{25a}$$

$$\left(\sum_e\mathbf{K}^e + \lambda_{cr}\sum_e\mathbf{K}_G^e\right)\boldsymbol{u} = 0 \tag{25b}$$

Eq. (25a) has a variable $\mathrm{s}_q^T = \sum_e \mathrm{s}_{qe}^T$, by solving this equation, we obtain phase-field $\boldsymbol{s}_q$ at the cracks.

Eq. (25b) is used to find critical loads λ_{cr} of the plate, however, due to stiffness matrices $\mathbf{K}^e$, $\mathbf{K}_G^e$ depending on phase-field variable $\boldsymbol{s}_q$, therefore, firstly, phase-field $\boldsymbol{s}_q$ variable of layer q (q=1-N) according to the corresponding mesh as shown in Figs. 2-4 (assuming that the plate contains three layers) through Eq. (25a) is processed. Then the values of $\boldsymbol{s}_q$ will be substituted in Eq. (22) to determine the stiffness matrices through the general mesh for the whole plate (see Fig. 5) with the specified $\boldsymbol{s}_q$ values. Next, the critical loads and buckling mode shapes of the structure can be obtained from Eq. (25b).

To calculate $\boldsymbol{s}_q$ of layer q, the crack shape in each layer is defined by solving Eq. (25a) with function $\Psi_q(\boldsymbol{u})$ based on the coordinates of this crack as follow [18,19,29]

$$\Psi_q(\boldsymbol{u}) = B\frac{G_C^q}{4l}.H_q(x) \tag{26a}$$

where

$$H_q(x) = \begin{cases} 1 & if\, x \le c_q\, and\, \frac{-l_0}{2} \le y \le \frac{l_0}{2} \\ 0 & else \end{cases} \tag{26b}$$

herein c_q is the crack length in layer q, the higher the scalar B's magnitude is the better, in this work its can be gotten $B = 10^3$, see detailly in Table 2. Normally, G_C^q is a material parameter and determined through a material homogenization

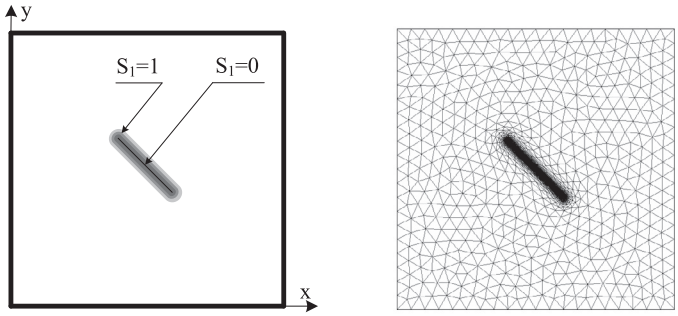

Fig. 2. The crack model in layer 1 of the composite plate.

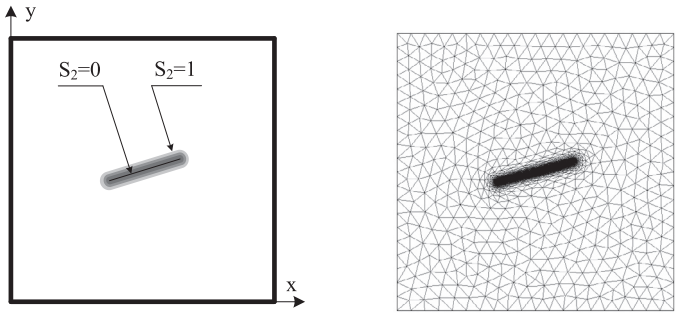

Fig. 3. The crack model in layer 2 of the composite plate.

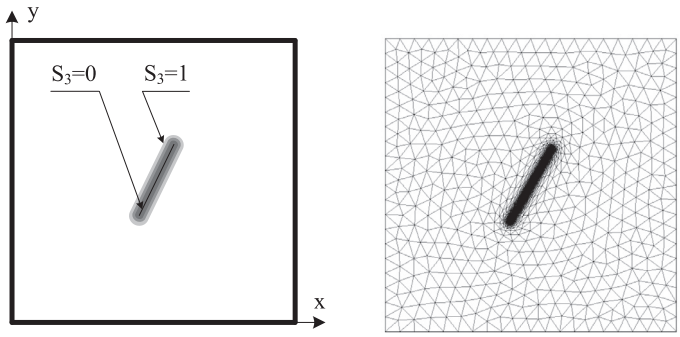

Fig. 4. The crack model in layer 3 of the composite plate.

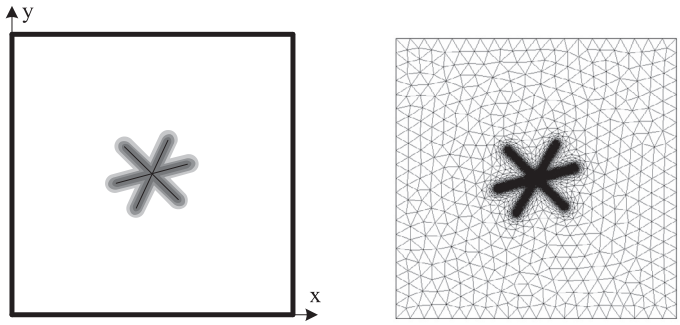

Fig. 5. The general model of three cracks of the composite plate with three layers.

Table 1
The present results are compared with those of other results for buckling load of composite plate.

Angle-ply	This work				[26]	[27]
	1200 elements	1500 elements	5500 elements	7000 elements		
$(0^0, 0^0, 0^0)$	2.381	2.370	2.363	2.362	2.39	2.391
$(15^0, -15^0, 15^0)$	2.451	2.442	2.426	2.425	2.45	2.448
$(30^0, -30^0, 30^0)$	2.579	2.565	2.559	2.558	2.57	2.578
$(45^0, -45^0, 45^0)$	2.651	2.643	2.629	2.627	2.64	2.649
$(0^0, 90^0, 0^0)$	2.398	2.386	2.364	2.362	2.39	2.394

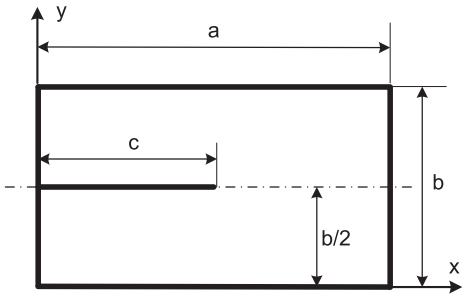

Fig. 6. The geometric model of a plate with an edge crack.

process based on the G_C^q value of the material components. In this work,G_C^q is determined depending on the material properties and it has important implications in crack propagation problems due to the value of G_C^q determines the load capacity before the crack spreads. However, in this problem, the authors do not take into account the propagation capacity of the crack, and G_C^q is used only in Eq. (26) to determine the shape of the crack according to the methods proposed in the works [18,19,29]. Accordingly, $\Psi_q(\boldsymbol{u})$ is chosen as Eq. (26a) to ensure $\Psi_q(\boldsymbol{u}) >> G_C^q$. This selection guarantees $s_q = 0$ in the area defined by $H_q = 1$ in Eq. (26b). Note that Eq. (26b) is only used to define straight cracks, however, for cracks with complex shapes, it is necessary to use the Level set function as shown in the reference [29].

***Remark**:* Throughout this proposed theory, in order to be convenient, the formula of one crack is established in the angle-ply direction of each laminated layer. Nevertheless, the expansion of the problem with multiple cracks and the direction of cracks can be freely changed by defining the function H_q in Eq. (26b).

3. Numerical results

Herein, in the following investigations, some boundary conditions are used and described as follows: S represents a simply supported edge, C represents a clamped edge, and F represents a free edge. So, a fully 4-edge simply supported plate is SSSS, and a fully 4-edge clamped supported plate is CCCC.

The plate is simply supported at $x = 0$, *a:* $v_0 = w = \varphi_y = 0$

The plate is simply supported at $y = 0$, *b:* $u_0 = w = \varphi_x = 0$

The plate is clamped at any edges: $u_0 = v_0 = w = \varphi_x = \varphi_y = 0$

The plate is free at any edges, no degrees of freedom are fixed.

3.1. Comparison

A laminated square plate has the dimension: length a, width b with $a = b =$ 10m, the thickness [26,27] $h =$ 0.06m, this plate is fully simply supported (SSSS). The plate material parameters of E-glass/epoxy are employed $E_1/E_2 = 2.45$, $G_{12} = 0.48E_2$, $\nu_{12} = 0.23$, $\nu_{21} = \nu_{12}E_2/E_1$; the plate is subjected to the compressive load in the x-axis. The buckling critical load is defined as [26,27]

$$k = \lambda_{cr} a^2/\pi^2 D_0 \tag{27}$$

where $D_0 = E_1 h^3/(12(1 - \nu_{12}\nu_{21}))$

The buckling critical loads of the three-layer composite plate in this work are compared with those of the mesh-free method [26,27] as presented in Table 1. It can be seen that both two methods have good agreement. In this comparison, a mesh with a number of elements from 1200 to 7000 elements is used.

Next, the critical buckling temperature rise (CBTR) of a cracked plate depicted in Fig. 6 is examined, this plate has four boundary conditions: fully clamped (CCCC), full 4-edge simply supported (SSSS), 2 edges are simply supported and the other two edges are free (SFSF), the two opposite sides are clamped and the two remaining edges are simply supported (SCSC). This plate is made from Al_2O_3 (Young's modulus E =380 GPa, Poisson's ratio 0.3, the coefficient of thermal expansion 74.10^{-7}

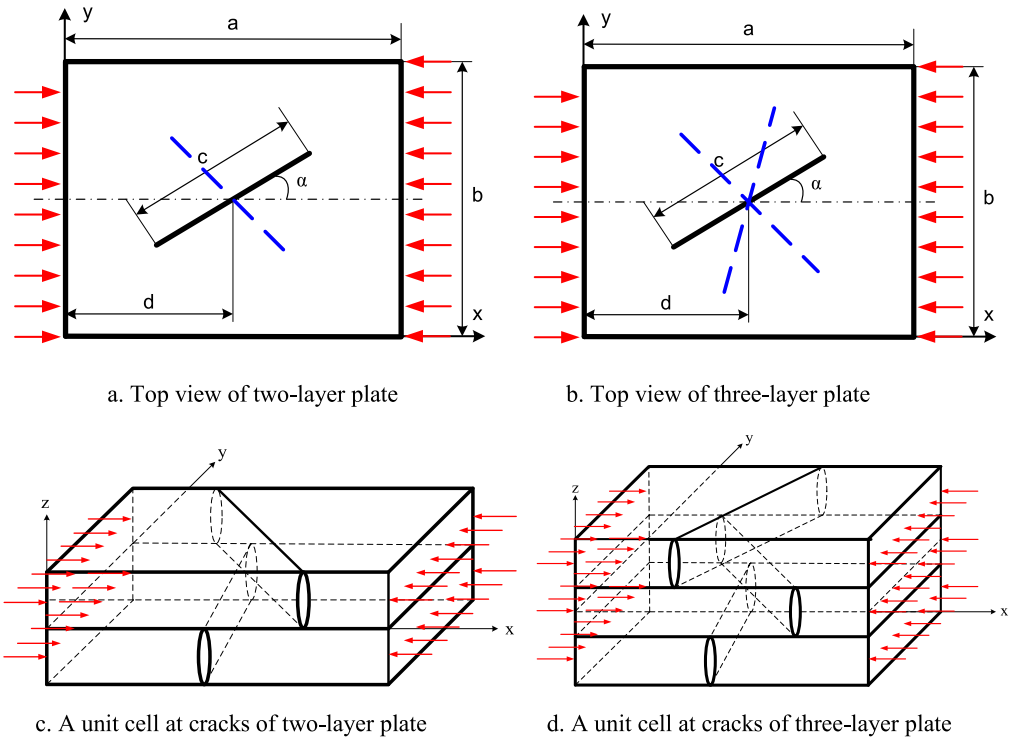

Fig. 7. The model geometry of a cracked composite plate.

Table 2
Comparison of the CBTR of a rectangular Al_2O_3 plate (c/a=0.5, a = 2m, b=1m, h/b = 0.01).

Method			The boundary conditions			
			CCCC	SCSC	SSSS	SFSF
XIGA [28]			17.036	14.415	6.225	1.960
This work	B=10^3	1200 elements	17.521	14.763	6.316	1.987
		1500 elements	17.396	14.619	6.237	1.979
		5500 elements	17.180	14.529	6.170	1.960
		7000 elements	17.179	14.526	6.168	1.959
	B=10^4	7000 elements	17.178	14.525	6.164	1.950
	B=10^4	7000 elements	17.178	14.525	6.164	1.950

1/°C) with a = 2m, b = 1m, thickness $h = b/100$, crack length $c = a/2$. The present results and the data from XIGA method [28] are compared. The similarity between those data can be seen in Table 2. The mesh as in the comparison above is also used, from the computed results based on this mesh, it found that the mesh has 7000 elements that have a good convergence, so for the coming sections, this mesh is used. The value of parameter B in (26a) increases gradually from 10^3 to 10^5, when $B = 10^3$ has ensured the required precision so that in this work, its value was chosen.

Finally, the comparison of this work and experiment approach by Seifi. et al. [40] for the homogenous plate with one crack is carried out. Consider a square plate with a=240mm, the plate thickness 12mm, and Poisson's ratio 0.33. The plate is under the compressive load at two opposite clamped edges, the remaining edges are free. The comparative results are presented in Table 3, it can be seen that a largest difference between this work and experiment approach is 8.97 %. This is explained that the plate material is made not pure and the crack shape is not perfect. Therefore, it can be concluded that the proposed theory and mathematical model are reliable.

3.2. Numerical analysis

Based on the proposed theory and calculation program with the high accuracy to investigate the effect of several parameters on the buckling of cracked composite plates, a cracked composite plate with the ratio a/b=1, the thickness $h = a/100$ is now examined. This plate is made from a three-layer E-glass/epoxy with material characteristics and critical buckling loads described in the above section (section 3.1). The plate is compressed along the Ox axis as shown in Fig. 7, and the buckling critical load is defined in Eq. (27).

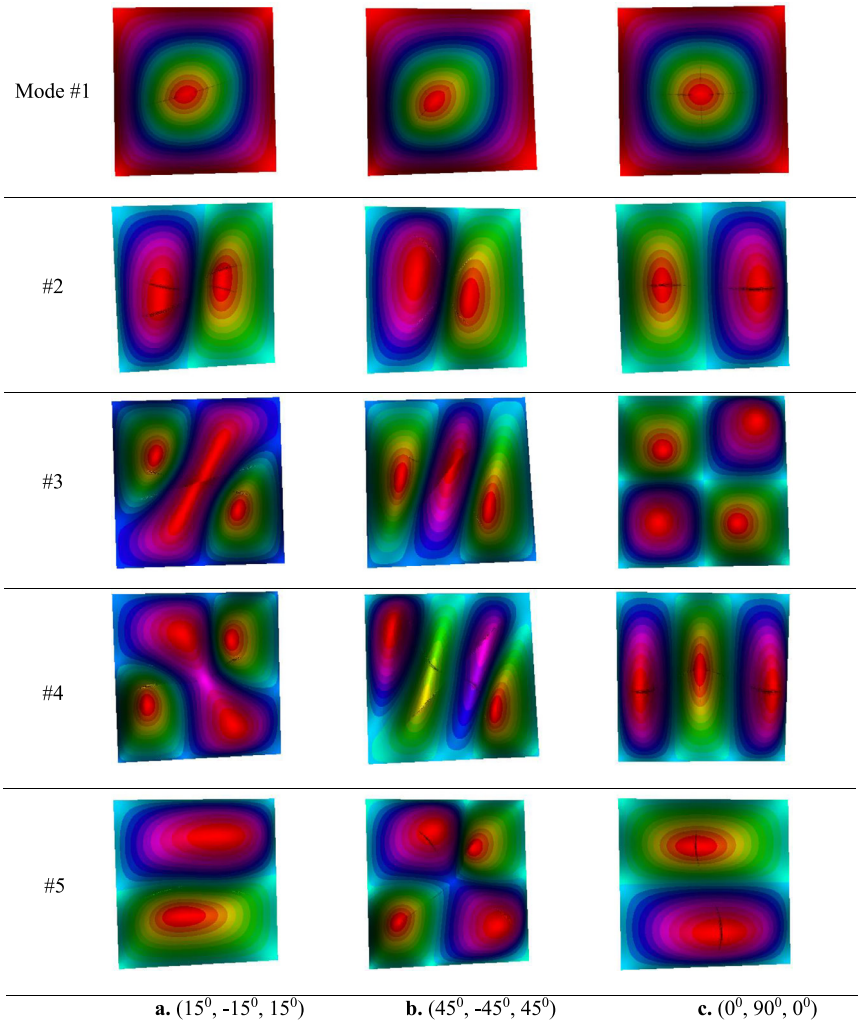

Fig. 8. Buckling mode shapes of cracked plate ($a = b = 0.2$m, $h = b/100$, $c/a = 0.8$, axial compression).

Table 3
Critical buckling load of cracked plate of present results are compared with experimental results.

Crack length (c/a)	Crack inclination (α)	Experimental buckling load (N) [40]	This work (N)	% Error
0.1	0	1627	1773	8.97
0.3		1531	1537	0.39
0.5		1317	1205	8.50
0.1	30^0	1651	1782	7.94
0.3		1551	1626	4.83
0.5		1396	1413	1.21
0.1	60^0	1674	1798	7.40
0.3		1660	1756	5.78
0.5		1636	1723	5.31

3.2.1. Buckling of cracked composite square plate

First of all, the effect of the length of the crack on the buckling of this plate is carried out. We suppose that the plate has different angle-plies among layers, the boundary condition is SSSS. Each layer has a crack in the center of the plate, and the length of each crack is represented as c. By changing c so that $c/a = 0.1$-0.8, $d = 0.5a$, the gotten numerical results are presented in Tables 4 and 5. Notice that the buckling load is computed as Eq. (27).

It can be observed that when increasing the crack length, the critical load of the plate decreases (caused by the area of energy loss) when the compressed load increases. In consideration of the angle-ply orientations, the composite plate (45^0, -45^0,45^0) has the highest critical load, which can be explained that the combination of the layers of materials makes

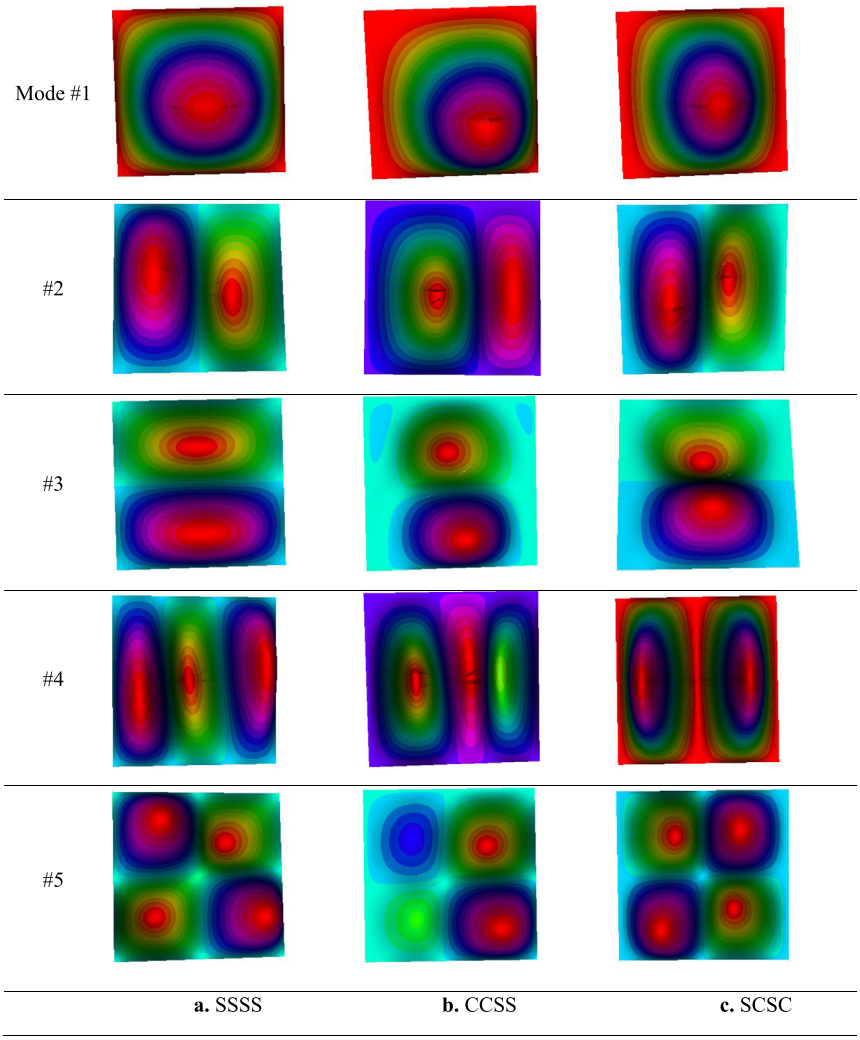

Fig. 9. Buckling modes of cracked (0^0, 30^0, 0^0) plate (a=b=0.2m, h=H/100, c/H=0.5, compressed along Ox axis.

Table 4
Effect of crack length on the critical buckling loads with various angle-ply orientations for the composite plate (axial compression).

	Angle-ply	*c/a*				
		0.1	0.3	0.5	0.6	0.8
Two layers	(0^0, 0^0)	2.33442	2.21871	2.07616	2.01489	1.93345
	(15^0, -15^0)	2.39736	2.36844	2.35099	2.34730	2.34985
	(30^0, -30^0)	2.52789	2.50200	2.48515	2.47888	2.47607
	(45^0, -45^0)	2.60281	2.57977	2.56029	2.55534	2.54846
	(0^0, 90^0)	2.30687	2.28426	2.27022	2.26713	2.26794
Three layers	(0^0, 0^0, 0^0)	2.33431	2.21853	2.07612	2.01484	1.93343
	(15^0, -15^0, 15^0)	2.40625	2.36771	2.34039	2.33288	2.33013
	(30^0, -30^0, 30^0)	2.54082	2.50792	2.48216	2.46969	2.46082
	(45^0, -45^0, 45^0)	2.61174	2.58287	2.55881	2.54726	2.53155
	(0^0, 90^0, 0^0)	2.34716	2.32169	2.30598	2.30573	2.30531

this plate stiffer. Fig. 8 presents the first five buckling mode shapes of the cracked composite plate with three angle-ply types. It can find that the angle-ply also has a great effect on critical forms of the cracked composite plate. For mode 1, the buckling mode shape changes slightly according to the angle-ply, however, buckling mode shapes changes clearly in higher frequencies. The reason is that when the cracks and angle-plies locate in different positions will cause the surface to release energy at those cracks according to the direction of the external force.

Table 5
Effect of crack length on the critical buckling loads with various angle-ply orientations for the composite plate (bi-axial compression).

Angle-ply		*c/a*				
		0.1	0.3	0.5	0.6	0.8
Two layers	(0^0, 0^0)	1.16689	1.09837	0.99585	0.94587	0.87338
	(15^0, -15^0)	1.19851	1.18313	1.17231	1.16929	1.16713
	(30^0, -30^0)	1.26375	1.25032	1.24085	1.23683	1.23346
	(45^0, -45^0)	1.30168	1.29018	1.28043	1.27797	1.27445
	(0^0, 90^0)	1.15359	1.14229	1.13528	1.13378	1.13414
Three layers	(0^0, 0^0, 0^0)	1.16682	1.09835	0.99582	0.94584	0.87333
	(15^0, -15^0, 15^0)	1.20304	1.18232	1.16598	1.16046	1.15520
	(30^0, -30^0, 30^0)	1.27051	1.25330	1.23897	1.23184	1.22423
	(45^0, -45^0, 45^0)	1.30598	1.29075	1.27965	1.27382	1.26595
	(0^0, 90^0, 0^0)	1.17359	1.16027	1.15136	1.14919	1.14898

Table 6
The dependence of the critical load on the d/a ratio (axial compression).

	Angle-ply	*d/H*				
		0.25	0.3	0.35	0.4	0.45
Two layers	(0^0, 0^0)	2.29836	2.27259	2.25025	2.23317	2.22246
	(15^0, -15^0)	2.40280	2.39202	2.38249	2.37487	2.37009
	(30^0, -30^0)	2.53617	2.52505	2.51552	2.50853	2.50382
	(45^0, -45^0)	2.61282	2.60259	2.59326	2.58598	2.58134
	(0^0, 90^0)	2.31506	2.30537	2.29674	2.28992	2.28568
Three layers	(0^0, 0^0, 0^0)	2.29831	2.27255	2.25020	2.23314	2.22242
	(15^0, -15^0, 15^0)	2.40833	2.39558	2.38426	2.37534	2.36977
	(30^0, -30^0, 30^0)	2.54712	2.53444	2.52389	2.51525	2.50984
	(45^0, -45^0, 45^0)	2.62009	2.60835	2.59792	2.58989	2.58470
	(0^0, 90^0, 0^0)	2.31617	2.30593	2.29708	2.29021	2.28773

Table 7
The dependence of the critical load on the d/a ratio (bi-axial compression).

	Angle-ply	*d/a*				
		0.25	0.3	0.35	0.4	0.45
Two layers	(0^0, 0^0)	1.14119	1.12745	1.11547	1.10614	1.10036
	(15^0, -15^0)	1.19776	1.19315	1.18907	1.18583	1.18389
	(30^0, -30^0)	1.26435	1.25960	1.25585	1.25315	1.25118
	(45^0, -45^0)	1.30319	1.29912	1.29553	1.29269	1.29076
	(0^0, 90^0)	1.15431	1.15068	1.14729	1.14454	1.14282
Three layers	(0^0, 0^0, 0^0)	1.14113	1.12740	1.11541	1.10612	1.10034
	(15^0, -15^0, 15^0)	1.20037	1.19476	1.19006	1.18572	1.18328
	(30^0, -30^0, 30^0)	1.27019	1.26475	1.26024	1.25657	1.25418
	(45^0, -45^0, 45^0)	1.30690	1.30223	1.29803	1.29469	1.29245
	(0^0, 90^0, 0^0)	1.17271	1.16887	1.16539	1.16250	1.16083

Next, the effect of the crack position is considered, at this time the ratio c/b is 0.3, d is the distance from the crack center to an edge, d/b = 0.25-0.5 is the ratio when taking the crack from the outer to the middle of the plate. The results of the critical load are shown in Tables 6 and 7, now it can be seen that when the center of the crack moves to the center of the plate, it becomes weaker, the critical load then decreases. It is explained that the closer the crack is to the center of the plate, where the most energy is concentrated on, the higher the energy release. Therefore, the plate becomes weaker, which will reduce the critical load of the plate. This also means that the closer a crack appears to the center of the plate, the working capacity of the plate decreases, reducing the efficiency of using these structures.

Next, the influence of the crack angle of only the core layer by maintaining the two outer layers is investigated. When the crack angle of the middle layer is changed in a range from 0^0-90^0, the numerical results obtained in Table 8 illustrates the critical load of cracked composite plates. Note that all 3 layers have cracks in the middle of the plate and along the core angle, and they have the following parameters: $c/a = 0.5$, $d = 0.5a$.

From Table 7, it can be seen that when the core angle of the middle layer (which is also the angle-ply of the crack) changes, the critical buckling does not change much. It means that the core angle has a small influence on the critical buckling. Fig. 9 shows the first five buckling mode shapes of the cracked plate (0^0, 30^0, 0^0) with three boundary conditions. When increasing the core angle of the middle layer from 0^0 to 90^0, due to the interaction of the direction of the compressive load with the crack, the crack will close with increasing degrees of this angle. That is, it will reduce the ability to release energy through cracks, the plate becomes "stiffer", the ability to withstand compressive loads better. This figure also shows

Table 8
The buckling critical load depends on core angle of the middle θ (axial compression).

	$(0^0, \theta, 0^0)$						
	$\theta = 0^0$	$\theta = 15^0$	$\theta = 30^0$	$\theta = 45^0$	$\theta = 60^0$	$\theta = 75^0$	$\theta = 90^0$
SSSS	2.0765	2.2804	2.2959	2.3078	2.3114	2.3136	2.3159
CSCS	4.9553	5.1715	5.1669	5.1555	5.1413	5.1291	5.1236
CCSS	3.5681	3.8319	3.8460	3.8577	3.8641	3.8647	3.8645
CCCC	6.0160	6.5149	6.5287	6.5415	6.5559	6.5667	6.5693

Table 9
Effect of E_1/E_2 on the critical buckling loads with various angle-ply orientations for the composite plate (axial compression).

Angle-ply		E_1/E_2					
		2	3	10	20	30	40
Two layers	$(0^0, 0^0)$	4.63086	5.64065	12.56361	22.36727	32.12146	41.83252
	$(15^0, -15^0)$	5.27019	6.33456	12.71214	20.61629	27.86826	34.75380
	$(30^0, -30^0)$	5.48440	6.78049	13.74525	21.83713	29.31867	36.56194
	$(45^0, -45^0)$	5.60434	7.04432	14.58589	23.15717	31.07989	38.76733
	$(0^0, 90^0)$	5.15027	6.04495	11.32270	17.89071	24.12532	30.23038
Three layers	$(0^0, 0^0, 0^0)$	4.63075	5.64064	12.56357	22.36716	32.12131	41.83270
	$(15^0, -15^0, 15^0)$	5.23123	6.33097	13.28312	22.60459	31.66835	40.59235
	$(30^0, -30^0, 30^0)$	5.45841	6.79482	14.24224	23.22166	31.59901	39.70167
	$(45^0, -45^0, 45^0)$	5.58396	7.04994	14.80757	23.77125	31.99443	39.93871
	$(0^0, 90^0, 0^0)$	5.18444	6.20987	13.15968	22.97820	32.74892	42.48029

Table 10
Effect of E_1/E_2 on the critical buckling loads with various angle-ply orientations for the composite plate (bi-axial compression).

Angle-ply		E_1/E_2					
		2	3	10	20	30	40
Two layers	$(0^0, 0^0)$	2.22266	2.70158	5.75414	8.01676	9.07154	9.96665
	$(15^0, -15^0)$	2.62841	3.15845	6.31151	10.08089	12.65124	14.70075
	$(30^0, -30^0)$	2.73865	3.38487	6.82039	10.72613	14.28785	17.71317
	$(45^0, -45^0)$	2.80249	3.52362	7.34420	11.78142	15.92670	19.96621
	$(0^0, 90^0)$	2.57533	3.02290	5.67104	8.97954	12.12555	15.20829
Three layers	$(0^0, 0^0, 0^0)$	2.22261	2.70157	5.75413	8.01673	9.07151	9.96662
	$(15^0, -15^0, 15^0)$	2.60623	3.15345	6.57913	10.92827	13.43825	15.81545
	$(30^0, -30^0, 30^0)$	2.72479	3.39173	7.07289	11.39925	15.3397	19.08894
	$(45^0, -45^0, 45^0)$	2.79225	3.52577	7.41743	11.93282	16.08583	20.09952
	$(0^0, 90^0, 0^0)$	2.58802	3.10107	6.57450	11.26424	14.37097	17.46874

that the buckling mode shapes of the plate do not differ much when the boundary conditions change, the difference only becomes more pronounced at higher frequencies. However, the buckling mode shapes differ greatly in their magnitude when the boundary conditions change, this is due to the different degrees of freedom are fixed, the stiffer will be changed. Therefore, it can see that the boundary conditions affect the buckling mode shapes of this plate.

Next, the effect of ratio E_2/E_1 is examined, the plate has a/b=1, a/h=100, $G_{12} = 0.48E_2$, $\nu_{12} = 0.23$, the buckling critical load is defined as

$$k = \lambda_{cr} a^2/\pi^2 D_1 \tag{28}$$

where $D_1 = E_2 h^3/(12(1 - \nu_{12}\nu_{21}))$

The plate is SSSS, c/a=0.5, $d = 0.5a$,$E_2 = 10^9$ N/m^2 is fixed. By increasing the ratio E_1/E_2 from 2 to 40, the obtained data are shown in Tables 9 and 10.

From Tables 9 and 10, it can see that when increasing the ratio E_1/E_2, the plate becomes stiffer, thus, the critical load of this plate also increases.

3.3. Buckling of cracked composite square plate with circular holes

In this last section, the behavior of the cracked composite plate with circular holes is investigated, this plate is SSSS. The parameters of the plate are given as follows: $a = b = 0.2$m, the holes have the same radius of $R = a/16$.

Next, to examine the influence of the plate thickness: consider the case where the plate has 4 holes at four corners (Fig. 10), by changing the thickness h of the plate so that $h = a/50$-$a/200$, the computing results of buckling load are shown as in Tables 11 and 12. It finds that when increasing the thickness, the plate becomes stronger, and its buckling load increases. Fig. 11 illustrates the first five buckling mode shapes of this plate with four holes in three cases of angle-ply ((0^0,

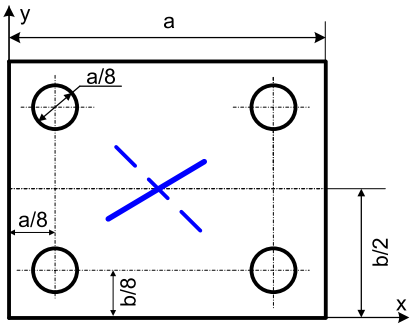

a. The model of two-layer plate with two cracks and four circle holes

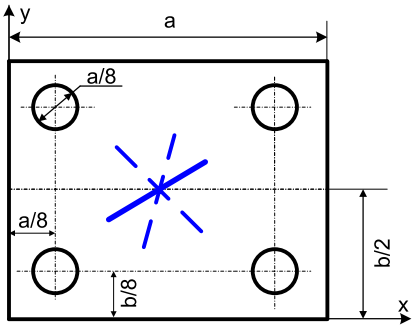

b. The model of three-layer plate with three cracks and four circle holes

Fig. 10. The cracked composite plate with holes.

Table 11
Effect of thickness h on the critical buckling loads with various angle-ply orientations for the composite plate (axial compression).

Angle-ply		*a/h*				
		50	100	150	180	200
Two layers	$(0^0, 0^0)$	15.82326	1.99559	0.59273	0.34335	0.25038
	$(15^0, -15^0)$	17.89092	2.24974	0.66769	0.38656	0.28185
	$(30^0, -30^0)$	18.67438	2.35107	0.69793	0.40416	0.29464
	$(45^0, -45^0)$	19.15271	2.41261	0.71637	0.41478	0.30240
	$(0^0, 90^0)$	17.37057	2.18269	0.64750	0.37482	0.27333
Three layers	$(0^0, 0^0, 0^0)$	15.82324	1.99553	0.59271	0.34332	0.25035
	$(15^0, -15^0, 15^0)$	17.83155	2.24269	0.66558	0.38537	0.28095
	$(30^0, -30^0, 30^0)$	18.75397	2.36140	0.70105	0.40598	0.29607
	$(45^0, -45^0, 45^0)$	19.27068	2.42753	0.72077	0.41734	0.30435
	$(0^0, 90^0, 0^0)$	17.66582	2.22016	0.65861	0.38134	0.27809

Table 12
Effect of thickness h on the critical buckling loads with various angle-ply orientations for the composite plate (bi-axial compression).

Angle-ply		*a/h*				
		50	100	150	180	200
Two layers	$(0^0, 0^0)$	7.61167	0.96166	0.28584	0.16559	0.12075
	$(15^0, -15^0)$	8.93184	1.12319	0.33328	0.19297	0.14066
	$(30^0, -30^0)$	9.33326	1.17490	0.34877	0.20190	0.14727
	$(45^0, -45^0)$	9.58309	1.20704	0.35832	0.20753	0.15133
	$(0^0, 90^0)$	8.69122	1.09207	0.32391	0.18756	0.13677
Three layers	$(0^0, 0^0, 0^0)$	7.61163	0.96160	0.28581	0.16554	0.12072
	$(15^0, -15^0, 15^0)$	8.89635	1.11884	0.33200	0.19225	0.14013
	$(30^0, -30^0, 30^0)$	9.37478	1.18038	0.35046	0.20297	0.14795
	$(45^0, -45^0, 45^0)$	9.64342	1.21479	0.36067	0.20883	0.15227
	$(0^0, 90^0, 0^0)$	8.82909	1.10951	0.32915	0.19059	0.13894

Table 13
Effect of number of the circular holes on the critical buckling loads with various angle-ply orientations for the composite plate (axial compression)

Angle-ply		*The number of the circle hole*				
		0	1	2	3	4
Two layers	(0^0, 0^0)	2.07615	2.05628	2.03606	2.01577	1.99554
	(15^0, -15^0)	2.35097	2.32559	2.30023	2.27494	2.24977
	(30^0, -30^0)	2.48478	2.45052	2.41795	2.38456	2.35104
	(45^0, -45^0)	2.56143	2.52334	2.48668	2.44928	2.41266
	(0^0, 90^0)	2.27022	2.24829	2.22663	2.20443	2.18263
Three layers	(0^0, 0^0, 0^0)	2.07613	2.05622	2.03601	2.01575	1.99551
	(15^0, -15^0, 15^0)	2.34035	2.31373	2.29189	2.26517	2.24266
	(30^0, -30^0, 30^0)	2.48217	2.44738	2.42105	2.38707	2.36145
	(45^0, -45^0, 45^0)	2.55884	2.52085	2.49344	2.45520	2.42754
	(0^0, 90^0, 0^0)	2.30599	2.28440	2.26303	2.24152	2.22011

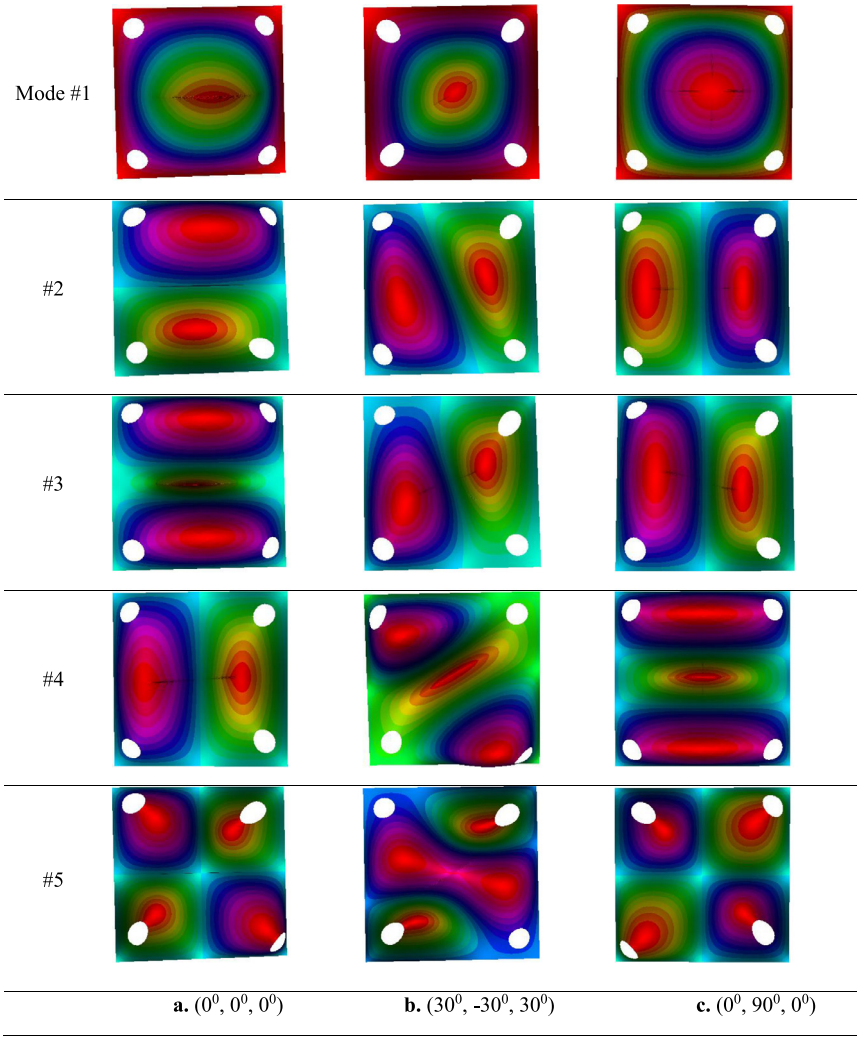

Fig. 11. Buckling modes of SSSS cracked plate (a=b=0.2m, h=a/100, c/a=0.5, bi-axial compression).

0^0, 0^0), (30^0, -30^0, 30^0), and (0^0, 90^0, 0^0)). One can see the combination of holes and angle-ply affect strongly the buckling mode shapes of the plate. This is explained by the fact that the energy-releasing surface of the plate at the position of the cracks varies with the direction of the compressive force, where the most obvious difference of the buckling mode shapes is shown at the 2^{nd}, 3^{rd}, and 4^{th} frequencies.

Next, the influence of the number of holes is carried out. To clarify the effect of the holes on the behavior of this plate, we consider four cases: the plate has one hole, the plate has two holes, the plate has three holes (Fig. 12), and the plate has

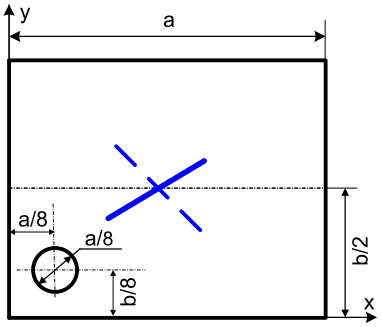

a. The model of two-layer plate with one hole

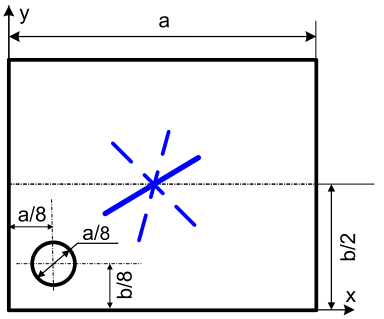

b. The model of three-layer plate with one hole

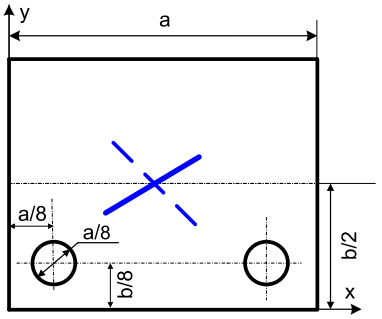

c. The model of two-layer plate with two holes

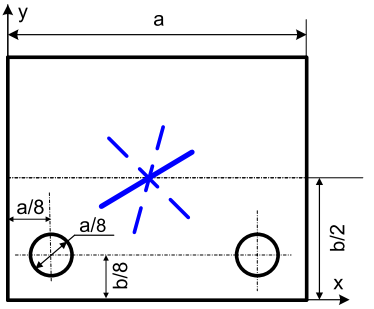

d. The model of three-layer plate with two holes

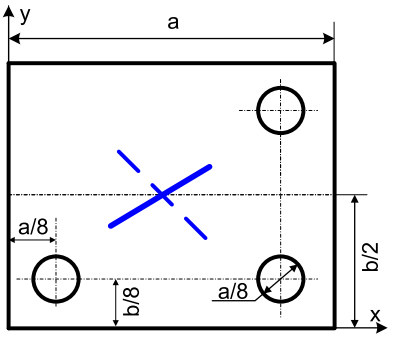

e. The model of two-layer plate with three holes

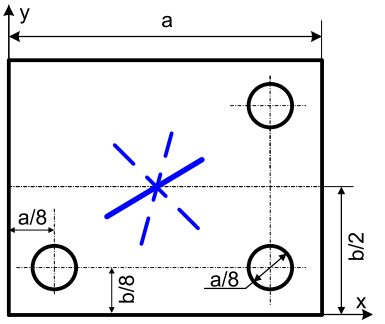

f. The model of three-layer plate with three holes

Fig. 12. The multi-holes cracked composite plate.

Table 14
Effect of number of the circular holes on the critical buckling loads with various angle-ply orientations for the composite plate (bi-axial compression).

Angle-ply		*The number of the circle hole*				
		0	1	2	3	4
Two layers	$(0^0, 0^0)$	0.99587	0.98733	0.97869	0.97015	0.96166
	$(15^0, -15^0)$	1.17233	1.16006	1.14753	1.13547	1.12310
	$(30^0, -30^0)$	1.24065	1.22387	1.20756	1.19144	1.17495
	$(45^0, -45^0)$	1.28090	1.26211	1.24349	1.22535	1.20709
	$(0^0, 90^0)$	1.13524	1.12448	1.11353	1.10282	1.09206
Three layers	$(0^0, 0^0, 0^0)$	0.99584	0.98730	0.97862	0.97011	0.96162
	$(15^0, -15^0, 15^0)$	1.16596	1.15323	1.14239	1.12985	1.11884
	$(30^0, -30^0, 30^0)$	1.23899	1.22246	1.20903	1.19304	1.18039
	$(45^0, -45^0, 45^0)$	1.27961	1.26107	1.24705	1.22892	1.21474
	$(0^0, 90^0, 0^0)$	1.15135	1.14089	1.13023	1.11997	1.10955

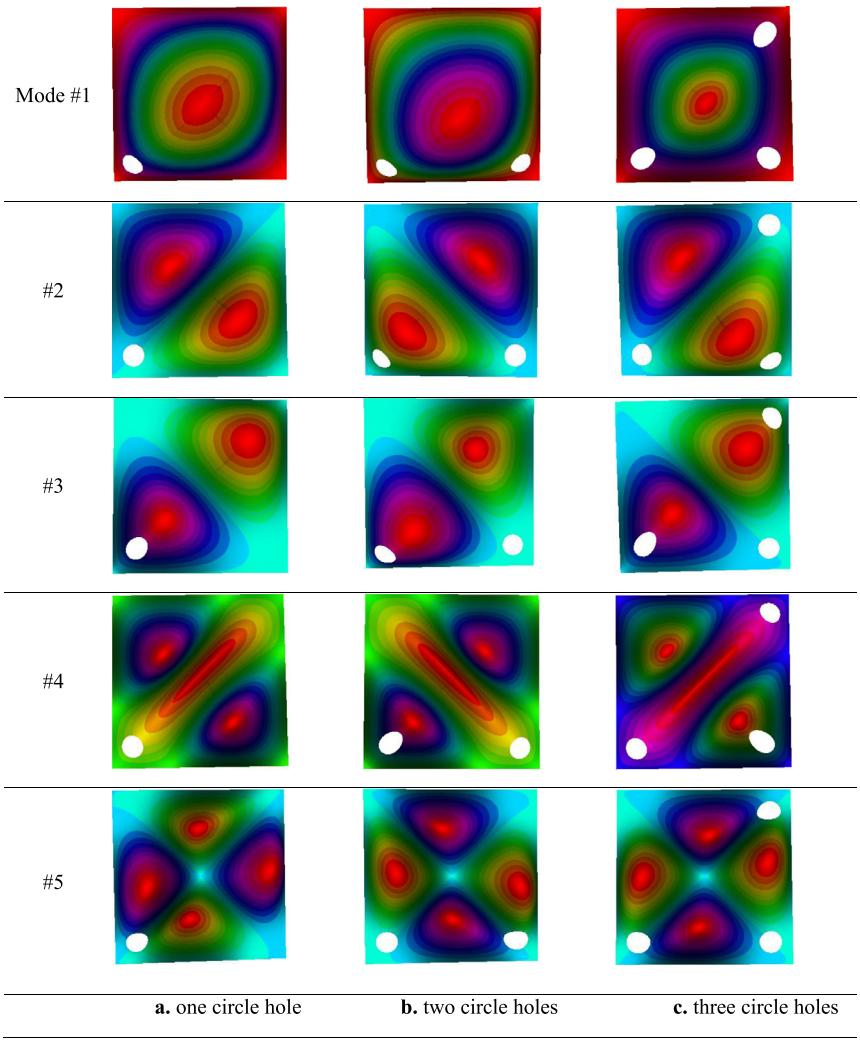

Fig. 13. Buckling modes of SSSS cracked plate (a=b=0.2m, h=a/100, c/a=0.5, (45^0, -45^0, 45^0), bi-axial compression).

four holes (Fig. 10), the computed results of the buckling load are listed in Tables 13 and 14. Looking at the data shown in those tables it finds that when increasing the number of holes, the structure becomes softer, and buckling load decreases. Fig. 13 shows the first five buckling mode shapes, it can be observed that the number of holes affects both the buckling as well as the mode shapes of this plate.

4. Conclusions

This paper presented the buckling analysis of multiple transverse cracking ply plates using first-order shear deformation theory and multi-phase-field theory. To conclude, some novel findings are highlighted as follows:

- This work successfully developed the finite element formulations in order to calculate the buckling problem of the laminated plate with multiple cracks along the angle-ply of each layer based on the first-order shear deformation theory and multi-phase-field theory. This proposed theory can be easily extended to investigate static bending and vibration, etc., of related mechanical structures.
- The proposed theory were verified and applied to solve some problems for laminated composite plates with multiple cracks along the angle-ply of each layer.
- For further works, the present theory could to be applied in mechanical analyses of plates with multiple cracks along the angle-ply of each layer, sandwich plates and laminated plates with piezoelectric components, etc., to figure out novel explorations, orientations for material designs as well as processes of monitoring strengths of materials.

- This problem can be extended in the direction of applying multi-phase-field theory and layerwise theory to model laminated plate problems with multiple transverse cracking ply and delamination. In addition, the present approach in this paper can be applied to investigate the mechanical behaviors of composite plates with multi-ply cracks subjected to different types of external loads such as thermal load, mechanical-thermal-electrical load, and so on. Based on those types of loads, the stiffness matric, geometric stiffness matric, and nodal displacement vector can be added corresponding components.

Acknowledgments

DVT gratefully acknowledges the support of Vietnam National Foundation for Science and Technology Development (NAFOSTED) under grant number 107.02-2018.30.

References

[1] A. Milazzo, I. Benedetti, V. Gulizzi, An extended Ritz formulation for buckling and post-buckling analysis of cracked multilayered plates, Compos. Struct. 201 (2018) 980–994.
[2] N. Amir, M. Soheil, XFEM buckling analysis of cracked composite plates, Compos. Struct. 131 (2015) 333–343.
[3] S. Rahman, R. Milad, Buckling analysis of cracked laminated plates by domain decomposition method, Ships Offshore Struct. 14 (3) (2019) 331–339.
[4] K.O. Amit, Nonlinear buckling analysis of damaged laminated composite plates, J. Compos. Mater. 0 (0) (2019) 1–16.
[5] R. Joffe, A. Krasnikovs, J. Varna, COD-based simulation of transverse cracking and stiffness reduction in [S/90n]s laminates, Compos. Sci. Technol. 61 (5) (2001) 637–656.
[6] D.H. Li, X. Zhang, K.Y. Sze, Y. Liu, Extended layerwise method for laminated composite plates with multiple delaminations and transverse cracks, Comput. Mech. 58 (2016) 657–679.
[7] X. Lu, Y. Yang, D. Xu, Y.G. Wu, L.i. DH, Extended Layerwise/Solid-Element method of composite sandwich plates with damage, Mech. Adv. Mater. Struct. 26 (2019) 1376–1389.
[8] D.H. Li, X. Yang, R.L. Qian, D. Xu, Static and dynamic response analysis of functionally graded material plates with damage, Mech. Adv. Mater. Struct. 27 (2020) 94–107.
[9] D.H. Li, Y. Liu, X. Zhang, An extended Layerwise method for composite laminated beams with multiple delaminations and matrix cracks, Int. J. Numer. Methods Eng. 101 (6) (2015) 407–434.
[10] M. Yuan, Y. Yang, H. Zhao, Y. Wang, R. Li, B. Zhang, J. Chen, A novel trans-scale method for predicting mode I matrix crack density of composite laminates, Compos. Struct. 235 (2020) 111726.
[11] W. Lai, J. Gao, Y. Li, M. Arroyo, Y. Shen, Phase field modeling of brittle fracture in an Euler–Bernoulli beam accounting for transverse part-through cracks, Comput. Methods Appl. Mech. Eng. 361 (2020) 112787.
[12] Y.M. Han, H.T. Hahn, R.B. Croman, A simplified analysis of transverse ply cracking in cross-ply laminates, Compos. Sci. Technol. 31 (1988) 165–177.
[13] C.V. Singh, R. Talreja, Evolution of ply cracks in multidirectional composite laminates, Int. J Solids Struct. 47 (2010) 1338–1349.
[14] P.A. Carraro, M. Quaresimin, A stiffness degradation model for cracked multidirectional laminates with cracks in multiple layers, Int. J Solids Struct. 58 (2015) 34–51.
[15] H.D. Duc, Q.B. Tinh, N.D. Duc, F. Kazuyoshi, Hybrid phasefield simulation of dynamic crack propagation in functionally graded glass-filled epoxy, Compos. Part B 99 (2016) 266–276.
[16] A. Schluter, A. Willenbucher, C. Kuhn, R. Muller, Phase field approximation of dynamic brittle fracture, Comput. Mech. 54 (2014) 1141–1161.
[17] K. Shiva, P. Raghu, A. Rajagopal, J.N. Reddy, Nonlocal buckling analysis of laminated composite plates considering surface stress effects, Compos. Struct. 226 (2019) 111216.
[18] K. Josef, A. Marreddy, L.D. Lorenzis, G. Hector, R. Alessandro, Phase-field description of brittle fracture in plates and shells, Comput. Methods Appl. Mech. Eng. 312 (2016) 374–394.
[19] B. Bourdin, G.A. Francfort, J.J. Marigo, The variational approach to fracture, J. Elast. 91 (2008) 5–148.
[20] V.D. Thom, H.D. Duc, N.D. Duc, Q.B. Tinh, Phase-field thermal buckling analysis for cracked functionally graded composite plates considering neutral surface, Compos. Struct. 182 (2017) 524–548.
[21] H.D. Duc, Q.B. Tinh, V.D. Thom, N.D. Duc, A rate-dependent hybrid phase field model for dynamic crack propagation, J. Appl. Phys. 122 (2017) 115102 1-4.
[22] H.D. Duc, V.D. Thom, M.P. Phuc, N.D. Duc, Validation simulation for free vibration and buckling of cracked Mindlin plates using phase-field method, Mech. Adv. Mater. Struct. 0 (2018) 1–10.
[23] N.D. Duc, T.D. Truong, V.D. Thom, H.D. Duc, On the Buckling Behavior of Multi-cracked FGM Plates, in: Procceeding of the International Conference on Advances in Computational Mechanics, Lecture Notes in Mechanical Engineering, 2017, pp. 29–45.
[24] M.P. Phuc, V.D. Thom, H.D. Duc, N.D. Duc, The stability of cracked rectangular plate with variable thickness using phasefield method, Thin-Walled Struct. 129 (2018) 157–165.
[25] V.H. Nam, H.D. Duc, M.K. Nguyen, V.D. Thom, T.T. Hong, Phase-field buckling analysis of cracked stiffened functionally graded plates, Compos. Struct. 217 (2019) 50–59.
[26] G.R. Liu, Mesh-free methods: moving beyond the finite element method, CRC Press, U.S.A., 2003.
[27] Q.B. Tinh, Buckling analysis of simply supported composite laminates subjected to an in-plane compression load by a novel mesh-free method, Vietnam J. Mech. 33 (2) (2011) 65–78.
[28] Y. Tiantang, Q.B. Tinh, Duc HD Shuohui, C.T. Wu, V.D. Thom, T. Satoyuki, On the thermal buckling analysis of functionally graded plates with internal defects using extended isogeometric anlysis, Compos. Struct. 136 (2016) 684–695.
[29] J.B. Michael, V.V. Clemens, A.S. Michael, J.R. Thomas, M.L. Chad, A phase-field description of dynamic brittle fracture, Comput. Methods Appl. Mech. Eng. 217–220 (2012) 77–95.
[30] Z. Peng, Y. Weian, H. Xiaofei, Q.B. Tinh, An explicit phase field model for progressive tensile failure of composites, Eng. Fract. Mech. (2020) 107371.
[31] P. Udit, P.T. Savvas, E. Yasser, MDLE. Federico, An anisotropic cohesive phase field model for quasi-brittle fractures in thin fibre-reinforced composites, Compos. Struct. 252 (2020) 112635.
[32] J. Wu, D. Wang, Z. Lin, D. Qi, An efficient gradient smoothing meshfree formulation for the fourth-order phase field modeling of brittle fracture, Comput. Particle Mech. 7 (2020) 193–207.
[33] L. Chen, B. Li, R.D. Borst, The use of Powell-Sabin B-Splines in a higher-order phase-field model for crack kinking, Comput. Mech. (2020).
[34] R. Ma, W.C. Sun, FFT-based solver for higher-order and multi-phase-field fracture models applied to strongly anisotropic brittle materials, Comput. Methods Appl. Mech. Eng. 362 (2020) 112781.
[35] A. Dean, A.V. Kumar PK, J. Reinoso, C. Gerendt, M. Paggi, E. Mahdi, R. Rolfes, A multi phase-field fracture model for long fiber reinforced composites based on the Puck theory of failure, Compos. Struct. 251 (2020) 112446.
[36] P. Raghu, A. Rajagopal, S.K. Jalan, J.N. Reddy, Modeling of brittle fracture in thick plates subjected to transient dynamic loads using a hybrid phase field model, Meccanica (2020) 1–18.

[37] G. Kikis, M. Ambati, L. De Lorenzis, S. Klinkel, Phase-feld model of brittle fracture in Reissner–Mindlin plates and shells, Comput Methods Appl. Mech. Eng. 373 (2021) 113490.
[38] J.N. Reddy, Mechanics of Laminated Composite Plates and Shells -Theory and Analysis, Second Edition, CRC Press, 2003.
[39] F. Amiri, D. Millan, Y. Shen, T. Rabczuk, M. Arroyo, Phase-field modeling of fracture in linear thin shells, Theor. Appl. Fract. Mech. 69 (2014) 102–109.
[40] R. Seifi, K.Y. Nafiseh, Experimental and numerical studies on buckling of cracked thin plates under full and partial compression edge loading, Thin-Walled Struct. 19 (2011) 1504–1516.